



Interferences in the re-emission field of multimodal leaky Lamb waves propagating in an immersed plate analytical modelling, simulation and experimentation

P. Kauffmann, Ma. Ploix, Jf. Chaix, C. Gueudre, G. Corneloup, F. Baque

► To cite this version:

P. Kauffmann, Ma. Ploix, Jf. Chaix, C. Gueudre, G. Corneloup, et al.. Interferences in the re-emission field of multimodal leaky Lamb waves propagating in an immersed plate analytical modelling, simulation and experimentation. Journal of Sound and Vibration, 2020, 10.1016/j.jsv.2019.115015 . cea-02339736

HAL Id: cea-02339736

<https://cea.hal.science/cea-02339736>

Submitted on 21 Dec 2021

HAL is a multi-disciplinary open access archive for the deposit and dissemination of scientific research documents, whether they are published or not. The documents may come from teaching and research institutions in France or abroad, or from public or private research centers.

L'archive ouverte pluridisciplinaire **HAL**, est destinée au dépôt et à la diffusion de documents scientifiques de niveau recherche, publiés ou non, émanant des établissements d'enseignement et de recherche français ou étrangers, des laboratoires publics ou privés.



Distributed under a Creative Commons Attribution - NonCommercial 4.0 International License

Title

Interferences in the re-emission field of multimodal leaky Lamb waves propagating in
an immersed plate: analytical modelling, simulation and experimentation

Authors' names and affiliations

Pierre KAUFFMANN^{1,2}, Marie-Aude PLOIX^{1,*}, Jean-François CHAIX¹, Cécile
GUEUDRE¹, Gilles CORNELOUP¹, François BAQUE²

¹ Aix Marseille Univ, CNRS, Centrale Marseille, LMA, Laboratoire de Mécanique et
d'Acoustique, Waves and Imaging group, Aix en Provence, France

² CEA Cadarache DEN/DTN/STCP/LISM (Laboratoire d'Instrumentation, Systèmes et
Méthodes), Saint Paul Lez Durance, France

*Corresponding author

Phone number: +33 (0) 4 42 93 90 84

E-mail address: marie-aude.ploix@univ-amu.fr

Postal Address: Laboratoire de Mécanique et d'Acoustique, CNRS - UMR 7031

Aix Marseille Université, IUT GMP

413 Avenue Gaston Berger

13 625 Aix en Provence Cedex 1

Abstract

The transmission and re-emission of energy by leaky Lamb waves from an immersed plate is being studied in the case of multi-modal propagation. When more than two Lamb modes propagate together, interferences can be generated in the re-emitted field. The latter have to be well understood and mastered because they can distort the diagnosis of a Non-Destructive Testing of an immersed plate. They are experimentally observed with C-scan visualisation, but they are not consistent with the Bertoni and Tamir model which describes the theoretical re-emitted acoustic field by leaky Lamb modes excited by an incident ultrasonic beam. The same interferences are also observed by finite-element simulation. The Bertoni and Tamir model is then modified to take into account the incidence of side lobes generated by an immersed ultrasonic transducer. That way, the same interferences observed are theoretically predicted, confirming that side lobes are the cause of it. Side lobes can generate a second leaky Lamb mode which propagate and interfere with the mode generated by the main acoustic beam. This secondary Lamb mode is non-negligible if it has higher leaky attenuation than the targeted mode. Thus, to avoid multi-modal generation with an incident beam, the best method is to aim at the leaky Lamb mode with the highest leaky attenuation coefficient at the chosen frequency.

Keywords

Leaky Lamb wave; re-emission; re-emitted field; transmitted field; leaky attenuation; interferences; multi-modal propagation

1. INTRODUCTION

The sodium-cooled fast reactor (SFR) technology has been chosen for the 4th generation of nuclear power plants in France. With liquid sodium as the coolant, improvement of in-service inspection and repair (ISI&R) techniques has been identified as a major issue for the ASTRID project (Advanced Sodium Technological Reactor for Industrial Demonstration) [1,2]. Ultrasonic solutions are being studied for the inspection of the main vessel and different internal parts of ASTRID: waves guided in elastic plates (Lamb waves) seem to be suitable candidates to achieve this objective [3,4]. The final objective of this work will be then to perform NDT in several parallel and immersed plates by using Lamb waves.

Lamb waves are frequently used for long-range non-destructive testing (NDT) of plates [5–10]. When the structure to be controlled is immersed in a fluid, Lamb waves leak energy into the surrounding fluid, which is why they are called leaky Lamb waves [10–14]. This is the case for the ASTRID main vessel filled with liquid sodium. To understand the physical phenomena occurring in such conditions, we decided to study the similar case of a stainless steel plate in water (given the wide diameter of the vessel, about 15 meters, we primarily choose to approximate it locally as a plate). In the case of a steel plate immersed in water, it has been shown that variations induced by the surrounding fluid on Lamb wave velocities are negligible [15]. However, leaky Lamb waves are highly attenuated, and this reduces the inspection range. To overcome this issue, we can use leaky Lamb modes with dominant longitudinal displacements and therefore with almost no leaky damping [16,17]. However, by reciprocity, these modes are particularly difficult to excite using a bounded-beam incident at a Lamb-wave generating angle [16].

The oblique incidence technique is widely used to generate leaky Lamb waves in an immersed plate: the required leaky Lamb mode is selected by the incidence of an acoustic beam generated by an immersed transducer or through a wedge [4,5,7,10,13,18–21]. This technique may result in the excitation of several leaky Lamb modes together because of the beam-spreading angle, thereby opening the door to multi-modal propagation [5].

In the case of multi-modal propagation, we can observe spatial interferences in the acoustic field emitted by the plate in the fluid [22–24]. Moreover, as a function of the defect, the creation of others Lamb modes can occur when the incident Lamb mode is reflecting on the defect. Thus, it can also lead to multi-modal propagation. The interferences in the re-emitted field could eventually complicate the diagnosis of NDT, and then they have to be well understood.

To compute the acoustic field reflected by and transmitted through a plate, an analytical model has been developed in reference [18], applied to the case of leaky Lamb waves in references [25,26], and numerically solved to take into account multi-modal propagation generated by the main incident beam in references [27,28]. This analytical model is referred to as the Bertoni and Tamir model in this paper. This model had never been used to study multi-modal interferences until now. The Bertoni and Tamir model takes into account the angle spreading of the acoustic beam, but it does not take into account the effect of side lobes inevitably generated by a real transducer. This effect has not been studied for the case of leaky Lamb waves, except in the recently published reference [29] which discusses finite-element simulations (FEM) of a complete acoustic field incident on a plate, but only for the normal incidence. We will show that side lobes can generate different leaky Lamb modes to that targeted by the

main beam under specific conditions, and we adapted the Bertoni and Tamir model in order to completely model all these phenomena.

In the first section, we present the general background of generation and re-emission of leaky Lamb waves, as well as the initial Bertoni and Tamir model. We experimentally highlight the presence of interferences in the re-emitted acoustic field in a configuration where the Bertoni and Tamir model does not predict any. Then, the Bertoni and Tamir model is modified to take into account the effect of side lobes on leaky Lamb mode generation. This clarifies the generation of leaky Lamb modes that lead to multi-modal propagation.

2. GENERATION AND RE-EMISSION: THEORETICAL AND EXPERIMENTAL

BACKGROUND

2.1. Generalities on generation, leakage and interferences

Lamb waves are generated in immersion with oblique incidence technique. For the sake of clarity, the same configuration is used in this paper and hereafter referred to as "our configuration": it refers to one stainless steel plate 7.8 mm thick, with an acoustic beam incident at an angle θ (different incidences will be tested), generated by a 500 kHz central frequency transducer (i.e. a product frequency x thickness of 3.9 MHz.mm) with an active diameter of 38.1 mm. Other numerical values that were used as input in the modelling are given in the appendix.

In order to visualize the experimental re-emitted field, Cscan acquisitions are performed and results are presented all along the paper. A picture of the experimental bench is shown in Figure 1. The transducer sends a wave train of 40 cycles at 500 kHz at the chosen incident angle θ . We choose a long wave train (40 cycles of sinusoid) because it is long enough to approximate the steady state. The transmitted field is

scanned and recorded by a needle hydrophone (\varnothing 0.5 mm) in the area perpendicular to the plate shown in dashed-dotted lines.

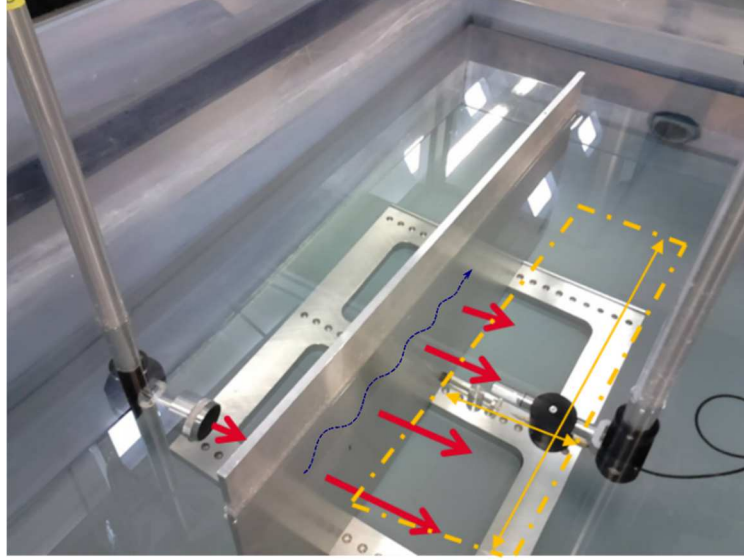


Figure 1: Experimental bench: incident bulk waves are sent by a transducer onto a plate immersed in water (7.8 mm thick and 700 mm long). Leaky Lamb waves are generated (symbolized by dashed blue arrow), and the transmitted acoustic field (bold red arrows) is scanned by a needle hydrophone in an area perpendicular to the plate (dash-dotted yellow line).

The plane wave reflection and transmission coefficients of the immersed plate are plotted as a function of the incident angle θ in Figure 2.a. These coefficients were calculated on the basis of reference [27] and will be applied later in the Bertoni and Tamir model. They provide a convenient way of visualising angles generating leaky Lamb modes that are characterised by a complete transmission and null reflection. Thus, in our configuration, S2 is generated at $\theta = 7.6^\circ$, S1 at $\theta = 15^\circ$, A1 at $\theta = 17.2^\circ$, S0 at $\theta = 29.5^\circ$ and A0 at $\theta = 31.3^\circ$.

Besides the leaky attenuation coefficient that quantifies leakage into the fluid [16] was calculated for each mode and is represented in Figure 2.b. It was calculated on the

basis of the formulation published in reference [12]. Its knowledge allows to provide for the level of re-emission of a mode, and by reciprocity the ability to generate a mode in the plate. For example, at 300 kHz, S0 presents the maximum of leaky attenuation coefficient and then will be the best mode available to be generated with oblique incidence technique. At the same time, it will be quickly attenuated along the plate and then will not be able to test long distance.

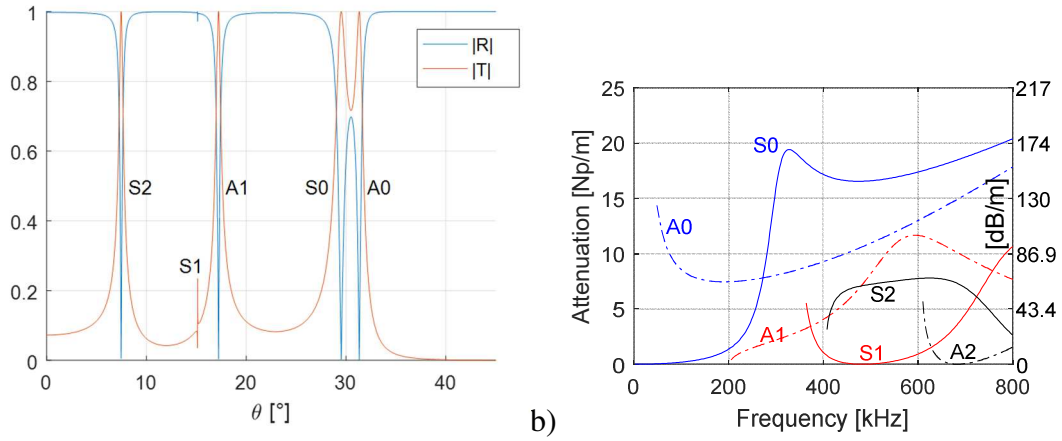


Figure 2: a) Theoretical reflection and transmission modulus at 500 kHz of the immersed stainless-steel plate as a function of the incidence angle θ . b) Theoretical leaky attenuation coefficient of Lamb modes for a stainless-steel plate with a thickness of 7.8 mm.

When a single mode is generated, the leakage along the plate is directed with the same angle as incident one [10-12]. When several modes are generated simultaneously in the immersed plate, their different leakages (with different directions) interfere with a constructive or destructive manner and can result in a new apparent leakage direction. The theoretical direction of these interference fringes for two different leaky Lamb modes (with directions θ_1 and θ_2) is given by equation 1 from references [23,24]:

$$\theta_s = -\arctan\left(\frac{\cos(\theta_2) - \cos(\theta_1)}{\sin(\theta_2) - \sin(\theta_1)}\right) \quad (1)$$

where θ_s is the direction of interferences, θ_1 and θ_2 the respective re-emission direction of leaky Lamb modes 1 and 2 that are propagating together.

2.2. The Bertoni and Tamir model

This part outlines the initial Bertoni and Tamir model. The model is then applied and compared to experimentation, and their limitations in our configuration are shown.

2.2.1. Principle

The Bertoni and Tamir model is an analytical model solved numerically to compute the reflected and transmitted steady state acoustical fields by an immersed plate. This model is extensively described in [27] and the same notations will be used, except for the half-width of the incident beam and its projection onto the plate that are noted r and r_0 respectively (instead of w and w_0) and the half-width spreading angle of the incident beam that is noted Θ_{HW} (instead of W_v).

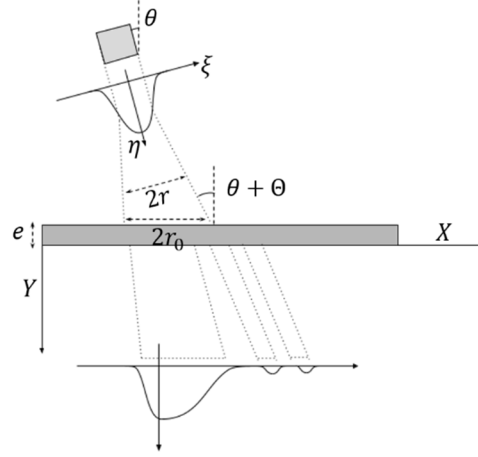
The plate is considered made of a homogeneous linear elastic isotropic medium. Coordinate systems are shown in Figure 3. The X and Y axes are associated with the plate (with X being parallel to the surface of the plate) and the ξ and η axis are linked with the incident acoustic beam (with ξ perpendicular to the incident acoustic beam). The incidence of the beam is centred on the angle θ , with a half-width spreading angle Θ (for which two definitions will be used, noted Θ_{HW} and Θ_0 , see below).

The Bertoni and Tamir model defines the incident acoustic field as a superposition of an infinite number of plane waves having the same wavelength but different incidence angles, through the following Fourier integral transforms [27]:

$$U_{inc}(X, Y) = \frac{1}{2\pi} \int_{k-\pi/r_0}^{k+\pi/r_0} V(k_X) \exp[i(Xk_X + Yk_Y)] dk_X \quad (2)$$

$$\text{and } V(k_X) = \int_{-r_0}^{r_0} U_{inc}(X, -e) \exp(-iXk_X) dX \quad (3)$$

177 with $k = 2\pi f/c$ the wave number in the liquid, c representing the speed of sound in the
 178 relevant liquid, f the frequency, k_x and k_y the components of k on the X and Y axes,
 179 and $U_{inc}(X, -e)$ the incident amplitude at the upper surface of the plate.



180
 181 Figure 3: An example of a transmitted beam profile with representation of the main acoustic
 182 beam spreading phenomena

183
 184 The propagation through the plate is then modelled by applying the plane wave
 185 reflection or transmission coefficients (please see [27] for detailed equations). We focus
 186 here on the way the incident beam is modelled. The incident beam is considered by the
 187 authors to have a gaussian distribution, with an angular spreading Θ . The definition and
 188 quantification of Θ may vary in the literature. We use two definitions:

- 189 ▪ Θ_{HW} which is defines in reference [27] as:

$$\Theta_{HW} = \sin^{-1}\left(\sin \theta + 0.53 c \cos \frac{\theta}{Df}\right) - \sin^{-1}\left(\sin \theta - 0.53 c \cos \frac{\theta}{Df}\right) \quad (4)$$

- 190 ▪ and Θ_0 as defined in equation (5) that gives the direction of the first zero amplitude
 191 enclosing the theoretical main beam [30,31]:

$$\Theta_0 = \sin^{-1}\left(1.22 \frac{c}{Df}\right) \quad (5)$$

192 with and D the diameter of the emitter.

193

The analytical expression of Gaussian beam incident at the upper surface of the plate ($Y = -e$) used in [27] is described in equation (6):

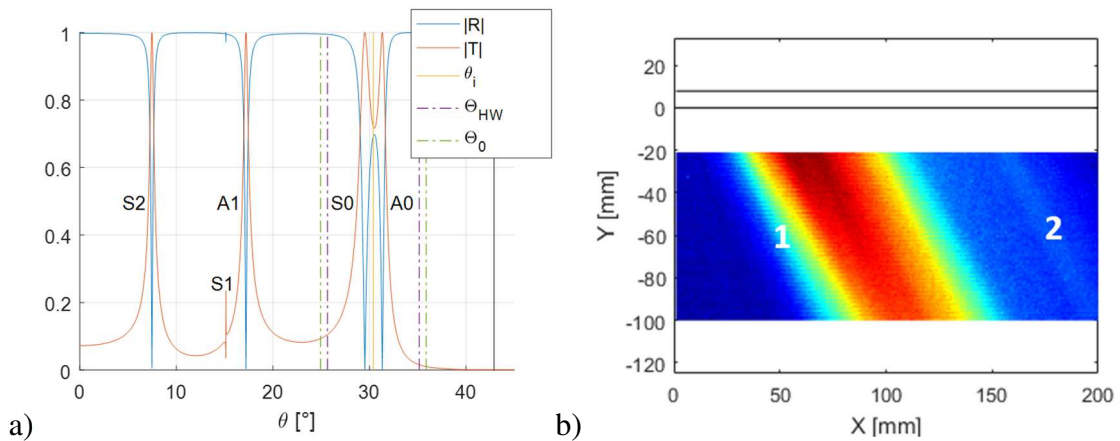
$$U_{inc}(X, -e) = \exp \left[-\left(\frac{X}{r_0} \right)^2 + iX \cdot k \cdot \sin(\theta) \right] \quad (6)$$

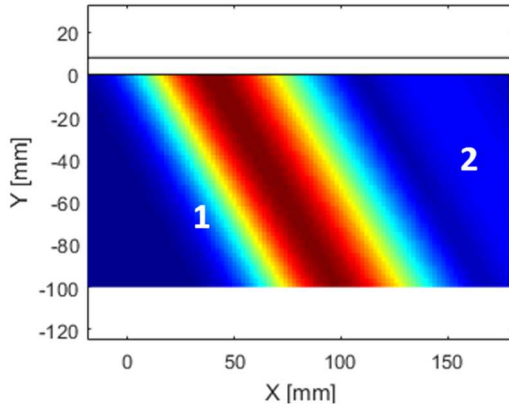
with $r_0 = r/\cos(\theta)$ the projection of the beam half-width on the plate as illustrated in Figure 3.

The equation (6) is then used as input: a spectral decomposition is applied, and the reflected or transmitted acoustic field is integrated using the plane wave reflection and transmission coefficients of the immersed plate that are presented in the Figure 2.a.

2.2.2. Comparison to experimental measurements

Experimentation with our configuration defined earlier, was performed with 30.4° incidence in order to generate both A0 and S0 by the main beam, as shown in Figure 4.a. One can observed one weak interference in the two acoustic fields presented, labelled 2 in the experimentation of Figure 4.b and in Bertoni and Tamir modelling in Figure 4.c: it is oriented at 30° , which is compatible with an interference between A0 and S0 according to equation (1). The experimentation is in good agreement with the Bertoni and Tamir model. Moreover, these results show that the Bertoni and Tamir model is able to predict interferences in the case of multimodal propagation.





c)

Figure 4: a) Reflection and transmission modulus with superposition of the main beam spreading angles Θ_{HW} and Θ_0 and incidence angles of side lobes for $\theta = 30.4^\circ$ at 500kHz. Comparison of the transmitted field: b) experimental C-scan, and c) Bertoni and Tamir model. The plate is illustrated by two parallel black lines and is immersed on both sides.

2.3. Limits of the model

Our configuration, this time with the incidence $\theta = 17.2^\circ$, implies the excitation of two Lamb modes by the main beam: A1 and S1 (see Figure 5.a). However, S1 presents zero re-emission at the working frequency of 500 kHz: its longitudinal displacements are predominant, inducing almost no leakage in the fluid [16,17]. This effect is highlighted by the null leaky attenuation coefficient of Figure 1.b. The zero attenuation of S1 at 500 kHz is clearly visible: this mode will almost induce no re-emission and by reciprocity will be hard to generate using an incident beam [16]. Therefore, the S1 mode will not have any influence in this case. Thus, only A1 should be generated considering only the main beam.

The C-scan image acquired in this case and represented in Figure 5.b reveals a stripped re-emitted acoustic field. At the very beginning of the acoustic field, a weak beam (labelled 1) is re-emitted around 9° . The main re-emission (labelled 2) is directed at around 18° , which is compatible with the re-emission of the A1 mode excited by the

main beam. However, the re-emission of strips soon occurs, directed between 23° and 25° (labelled 3).

Figure 5.c shows the transmitted field calculated by the initial Bertoni and Tamir model. We can observe the re-emission of the A1 mode which re-emits around 17° . The computed acoustic field is characteristic of the re-emission of a single leaky Lamb mode: one acoustic beam directed at a precise single angle, with an exponential decrease in the amplitude with propagation along the plate (example of Figure 5.d). It confirms that the contribution of the S1 mode has no measurable effect as expected.

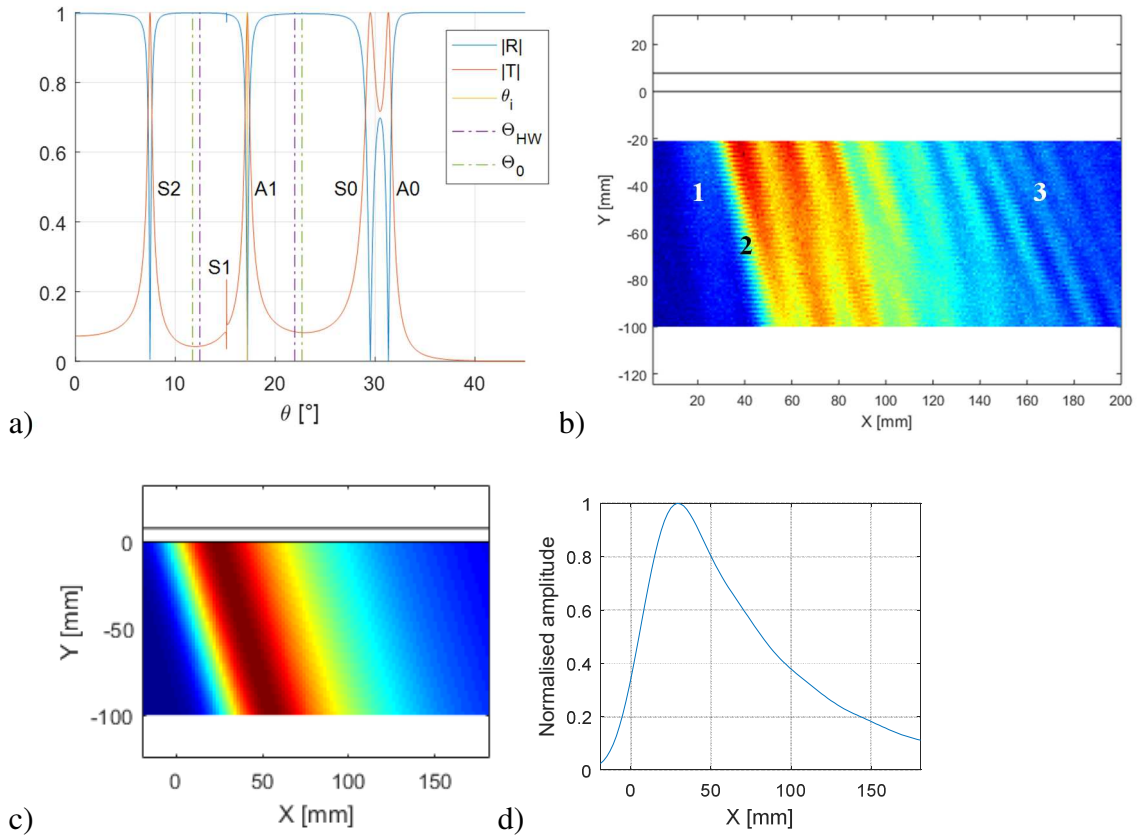


Figure 5: a) Reflection and transmission modulus with superposition of the main beam spreading angles Θ_{HW} and Θ_0 and incidence angles of side lobes for $\theta = 17.2^\circ$ at 500kHz. Comparison of the transmitted field: b) experimental C-scan, and c) Bertoni and Tamir model, with d) extracted normalised amplitude for $Y = -20$ mm.

However, the experimental and theoretical re-emitted acoustic fields are very different. This example highlights the necessity of taking into account the effect of side lobes in the modelling.

To ensure that experimentation is valid, we choose to confront it with finite elements simulation using the commercially available software COMSOL Multiphysics®. Calculations are made in the frequency domain to ensure the validity of the steady state hypothesis, which was made in the Bertoni and Tamir model. Since Lamb modes are purely 2D symmetrical, we use a 2D model to simplify and speed up our calculations. The transducer is classically modelled as a perfect piston source (with imposed pressure at its surface), which then generates a main beam and side lobes. Their characteristics were checked (near field length, and directions and amplitudes of the lobes) to match with our configuration.

Resulting reflected and transmitted field are represented in Figure 6. Perfectly matched layers (PML) were used to minimise reflections on the edges of the model. Some weak reflections still occur (because incidence angles on them are in the limits of their abilities) but they do not affect the part of interest.

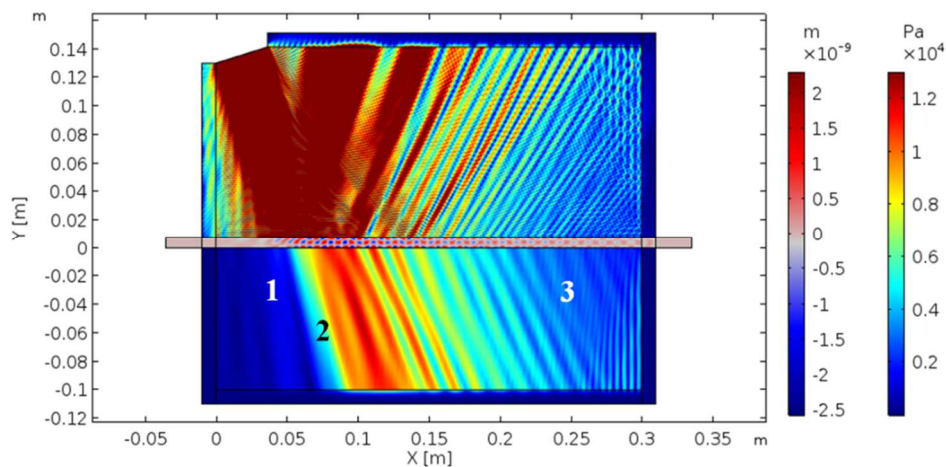


Figure 6: Transmitted acoustic field in our configuration computed with the FEM: the absolute pressure is plotted in water and vertical displacements in the plate

266

267 We can observe the same directions and interferences as in experimentation in the
268 transmitted field: the first direction (labelled 1) at a low amplitude at 9° , the main beam
269 (labelled 2) at 17.5° , and strips (labelled 3) oriented between 24° and 25° . This confirms
270 the experimentation results plotted in Figure 5.b, which lead to the conclusion that the
271 Bertoni and Tamir model is not relevant for this configuration. Since side lobes are
272 neglected in this model, we now modify the model to take them into account.

273

274 **3. MODIFICATION OF THE BERTONI AND TAMIR MODEL**

275 This part describes how side lobes were integrated in the Bertoni and Tamir model
276 and discuss several results compared to experimentations.

277 **3.1. Measurement of the experimental incident acoustic field**

278 For an accurate modelling of side lobes, we have chosen to measure the incident
279 acoustic field emitted by the transducer (500 kHz, \varnothing 38.1 mm). It is scanned with a
280 needle hydrophone (\varnothing 0.5mm). The signal is a wave train of 40 cycles at 500 kHz (the
281 same signal used for leaky Lamb wave experimentation). The resulting C-scan is shown
282 in Figure 7, where the red line represents the mean abscissa of the plate during
283 experimentation. The amplitudes measured on this line are plotted further in Figure 8.

284 Side lobes can be observed at -20 dB. The directions of the side lobes in Figure 7 are
285 12.5° , 20° and 26.5° for the first, second and third side lobe respectively. We then
286 model the amplitude and direction of these side lobes to take them into account in the
287 Bertoni and Tamir model.

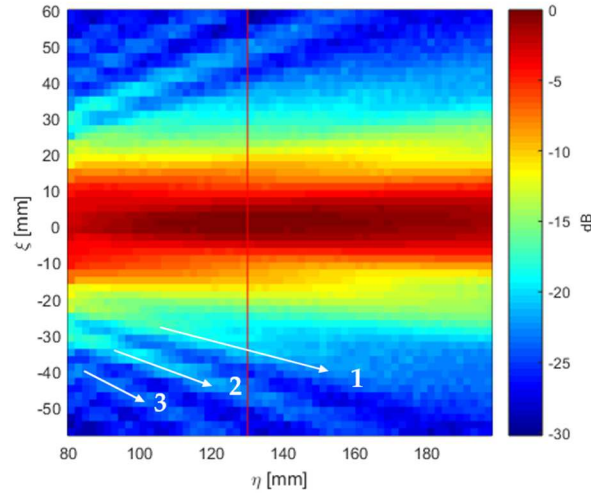


Figure 7: Experimental characterisation of the incident acoustic beam used in our configuration. The red line shows the near field length, representing also the mean abscissa where the plate is located during experimentation

3.2. Modeling of side lobes amplitude

Figure 8 shows that the Gaussian function used in Bertoni and Tamir model works well for the main beam but does not take into account the side lobes. To take them into account, we assessed two functions: the Bessel function of the first kind (its cardinal form is the theoretical cross section of an acoustic beam) in equation (7), and the Lorentz function in equation (8). Both of them were optimised with respect to the experimental data shown in Figure 8 using a least-squares method to approach the experimental conditions at best.

$$|U_{inc}(X, -e)| = \left| 2 \frac{J_1\left(\frac{\xi}{\beta}\right)}{\frac{\xi}{\beta}} \right| \quad (7)$$

with J_1 representing the Bessel function of the first kind, and β the parameter for optimisation which depends on the transducer, the frequency and the distance to the transducer. For our configuration, we have $\beta = 5.6$ mm.

$$|U_{inc}(X, -e)| = \frac{1}{1 + \left(\frac{\xi}{\gamma}\right)^2} \quad (8)$$

with γ representing the parameter for optimisation which depends on the transducer, the frequency and the distance to the transducer. For our configuration, $\gamma = 10.8$ mm.

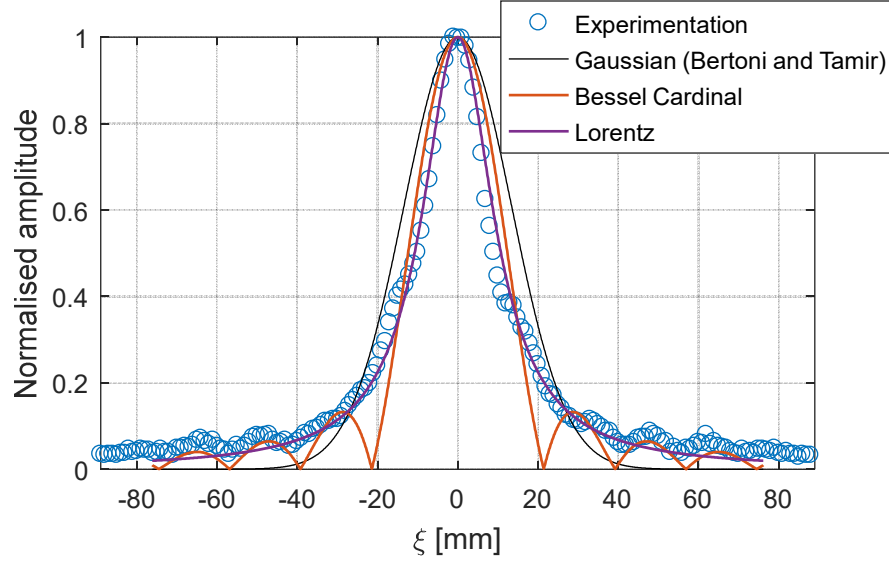


Figure 8: Incident acoustic beam profile with superposition of different model: the Bertoni and Tamir modelling (Gaussian) and optimised least-squares models (Bessel Cardinal and Lorentz functions)

The Bessel Cardinal function is able to well locate the side lobes and will be used to define angles (see next paragraph). However, it introduces zero values that are not experimentally measured. The Lorentz function appears to model the main beam and the mean amplitude of each side lobe quite well, which is why we chose it.

We have integrated the amplitude of side lobes using the Lorentz function into the modulus of $U_{inc}(X, -e)$ in the equation (9) below.

3.3. Modeling of side lobes directions

The incidence angle of the experimentally observed side lobes has to be taken into account into the phase of $U_{inc}(X, -e)$. To do so, we introduced a piecewise-defined function θ_n which returns the direction experimentally measured of the considered lobes as a function of the position in the ξ axis. The correspondence with the X axis was then easily obtained by a projection on the surface of the plate. The considered lobe itself was identified thanks to the zeros of the Bessel function. The first four zeros used are recalled in Table 1, with the corresponding angles experimentally measured and applied to the case of an incidence centred on θ . $\beta_0 = \beta/\cos(\theta)$ is used to take into account the projection on the surface of the plate illustrated in Figure 3.

X/β_0	$\theta_n(\frac{X}{\beta_0}) [^\circ]$
$ X/\beta_0 < 3.83$	θ
$3.83 \leq X/\beta_0 < 7.02$	$\theta + 12.5^\circ$
$7.02 \leq X/\beta_0 < 10.17$	$\theta + 20^\circ$
$10.17 \leq X/\beta_0 < 13.32$	$\theta + 26.5^\circ$

Table 1: Piecewise definition of θ_n for X positive. The definition of θ_n for X negative is based on the same scheme, with directions symmetrical to θ

The complete formulation of the incident acoustic field is presented in equation (9):

$$U_{inc}(X, -e) = \frac{1}{1 + \left(\frac{X}{\gamma_0}\right)^2} \cdot \exp \left[i \cdot X \cdot k \cdot \sin \left(\theta_n \left(\frac{X}{\beta_0} \right) \right) \right] \quad (9)$$

with $\gamma_0 = \gamma/\cos(\theta)$ and β_0 representing optimised parameters which depend on the transducer, the frequency and the distance to the transducer to the plate.

3.4. Results and discussion

3.4.1. At 500 kHz

The equation (9) was then used as input in the Bertoni and Tamir model. Numerical values used as input in the model are given in the appendix. The new results for the case of Figure 5 are given in Figure 9.

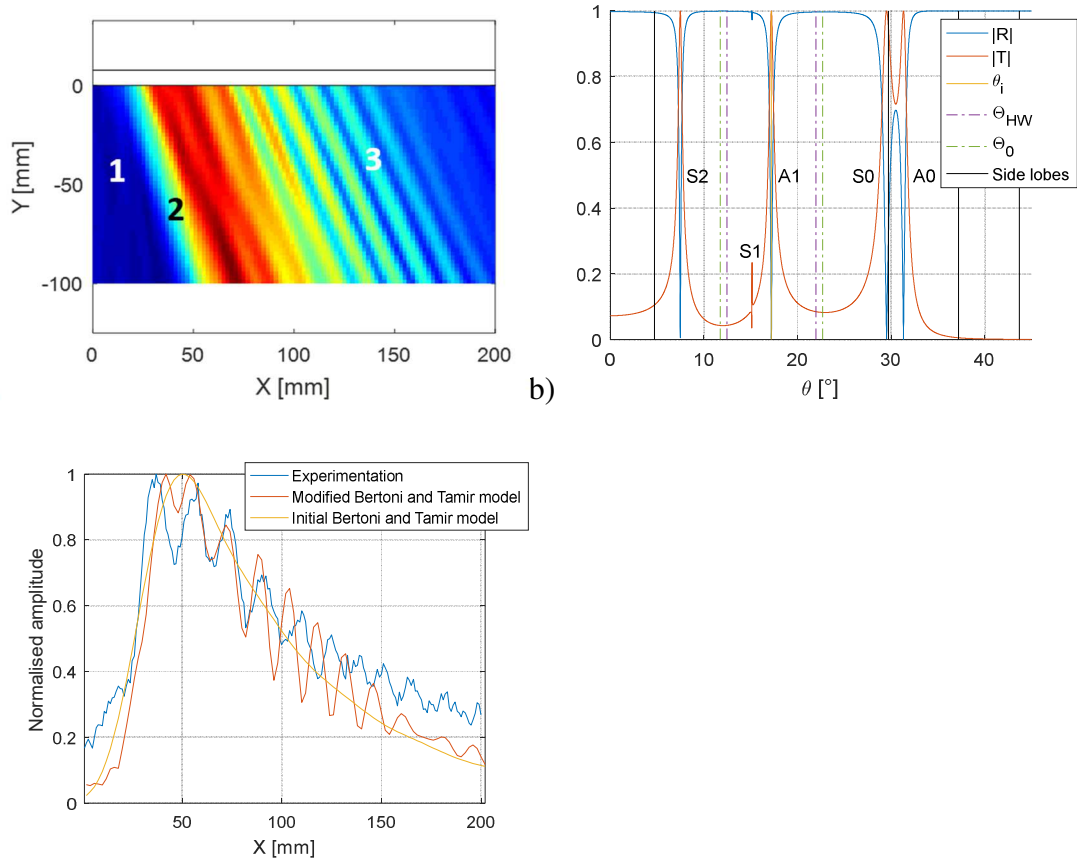


Figure 9: a) Transmitted acoustic field in our configuration computed with the modified Bertoni and Tamir model. b) Reflection and transmission modulus with superposition of the main beam spreading angles θ_{HW} and θ_0 and incidence angles of side lobes. c) Comparison of the amplitude at $Y = -20$ mm for the experimentation and the Bertoni and Tamir model with and without side lobes implementation.

The theoretical acoustic field in Figure 9.a reveals the same interferences than those observed experimentally and by FEM. At the very beginning of the acoustic field, a weak beam (labelled 1) is re-emitted around 9° , compatible with the re-emission of the S2 mode excited by the side lobe located left to the main beam (see incidences of side lobes in Figure 9.b). The main re-emission (labelled 2) was directed at around 17.5° , which is compatible with the A1 mode excited by the main beam. The side lobe on the right of the main beam excites A0 and/or S0 modes around 30° (theoretically 29.5° for S0 and 31.3° for A0). These modes propagate with A1 and these three modes are reemitting together, which creates interferences. These interferences are oriented between 24° and 25° (labelled 3).

Moreover, the theoretical direction of these interference fringes for two different leaky Lamb modes given by equation (1) results in $\theta_s = 23.4^\circ$ if considering S0 (with $\theta_1 = 17.2^\circ$ and $\theta_2 = 29.5^\circ$) and $\theta_s = 24.3^\circ$ if considering A0 (with $\theta_1 = 17.2^\circ$ and $\theta_2 = 31.3^\circ$), which is in very good agreement with experimentation, FEM and modified Bertoni and Tamir model.

S0 and/or A0 modes are excited with a weaker amplitude (-20 dB) in comparison to the excitation of A1, but their leaky attenuation coefficients are greater than A1 at 500 kHz (see Figure 2.b). This means that A0 and S0 are easier to excite with an incident beam and have a stronger re-emission than A1. This effect balances out the amplitude re-emitted by each mode and allows for non-negligible interferences.

The improvement of the model is highlighted by the extracted amplitudes at $Y = -20$ mm plotted in Figure 9.c. We can also note that a slight gap between the modified model and the experimental results tends to increase with the distance X . It can be partly explained by the fact that between labels 2 and 3, the interferences are not always

straight and probably indicate that more than two different Lamb modes are propagating together (probably A1, S2 and A0 and/or S0 in our configuration).

This proves that side lobes are indeed exciting A0 and/or S0 modes in the plate, inducing interference patterns in their re-emitted field in the fluid. This also underlines that side lobes cannot be neglected when incident at a highly attenuated Lamb mode and validates the way that the side lobes have been modelled. This point is confirmed by the other experimentations presented below.

Finally, the three different techniques used to study the transmitted field are brought together in Figure 10 and rescaled to simplify comparison. It can be seen that the directions and places of interference are in very good agreement between experimentation, FEM and the modified analytical model.

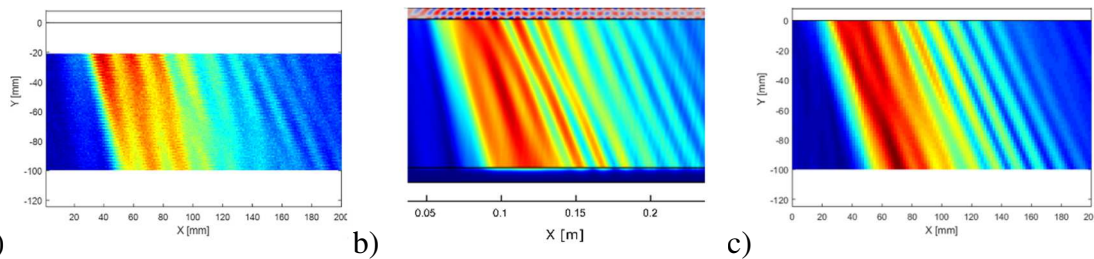


Figure 10: Comparison of the transmitted field on the same scale: a) experimental C-scan, b) finite-element simulation and c) modified analytical Bertoni and Tamir model

3.4.2. At 250 kHz

Other experimentations have been performed at 250 kHz with another transducer (\varnothing 46 mm, central frequency at 250 kHz) and compared to the results of the modified model. The new incident acoustic field has been characterised in Figure 11 with the same protocol as previously.

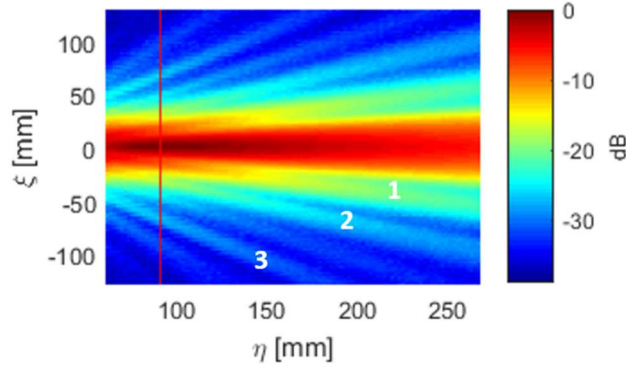


Figure 11: Experimental characterisation of the incident acoustic beam used at 250 kHz. The red line shows the near field length, representing the mean abscissa where the plate is located during experimentation

This leads to new values of the β and γ in equations (7) and (8): respectively 5.5 mm and 12.5 mm. The incidence of the first three lobes labelled in Figure 11 have been measured at 11.5° , 21° and 28° . These new parameters have been used as input of our modified Bertoni and Tamir model to take into account the incidence of side lobes.

Two different incidence angles are applied successively with this transducer: $\theta = 9^\circ$ to generate the A1 mode (Figure 12) and $\theta = 34.2^\circ$ to generate A0 (Figure 13).

The A1 mode (at $\theta = 9^\circ$) is the mode with the smallest leaky attenuation at 250 kHz (see Figure 2.b), which means that A0 and S0 modes will be easier to generate. The Figure 12.a shows that the S0 mode at 18.2° is at the extreme incidence of the main beam to be excited by it. However, this mode is likely to be excited by the first incident lobe, and the A0 mode (at 34.2°) by the second and the third incident lobe.

The initial Bertoni and Tamir model plotted in Figure 12.c predicts the re-emission of the only mode A1 at 9° (labelled 1) with a slow decrease along the plate because this mode is poorly attenuated. However experimentation (Figure 12.b) and modified Bertoni and Tamir model (Figure 12.d) reveals strong interferences, proving that other

modes are excited by side lobes. The first beam (labelled 1) is the re-emission of the A1
 mode at 9° . The second beam (labelled 2) is directed at 13.5° , which corresponds to the
 interference between A1 and S0 that is excited by the first side lobe: the equation (1)
 evaluates the interference at 13.6° . The third beam is measured at 18° and is the re-
 emission of the S0 mode without interference: the A1 mode has become negligible. The
 last double beam (labelled 4) is measured at about 25° , which is compatible with the
 interference between S0 mode and A0 predicted at 26.2° , the A0 mode being excited by
 the second and third side lobe. Experimentation and our modified Bertoni and Tamir
 model are in good agreement.

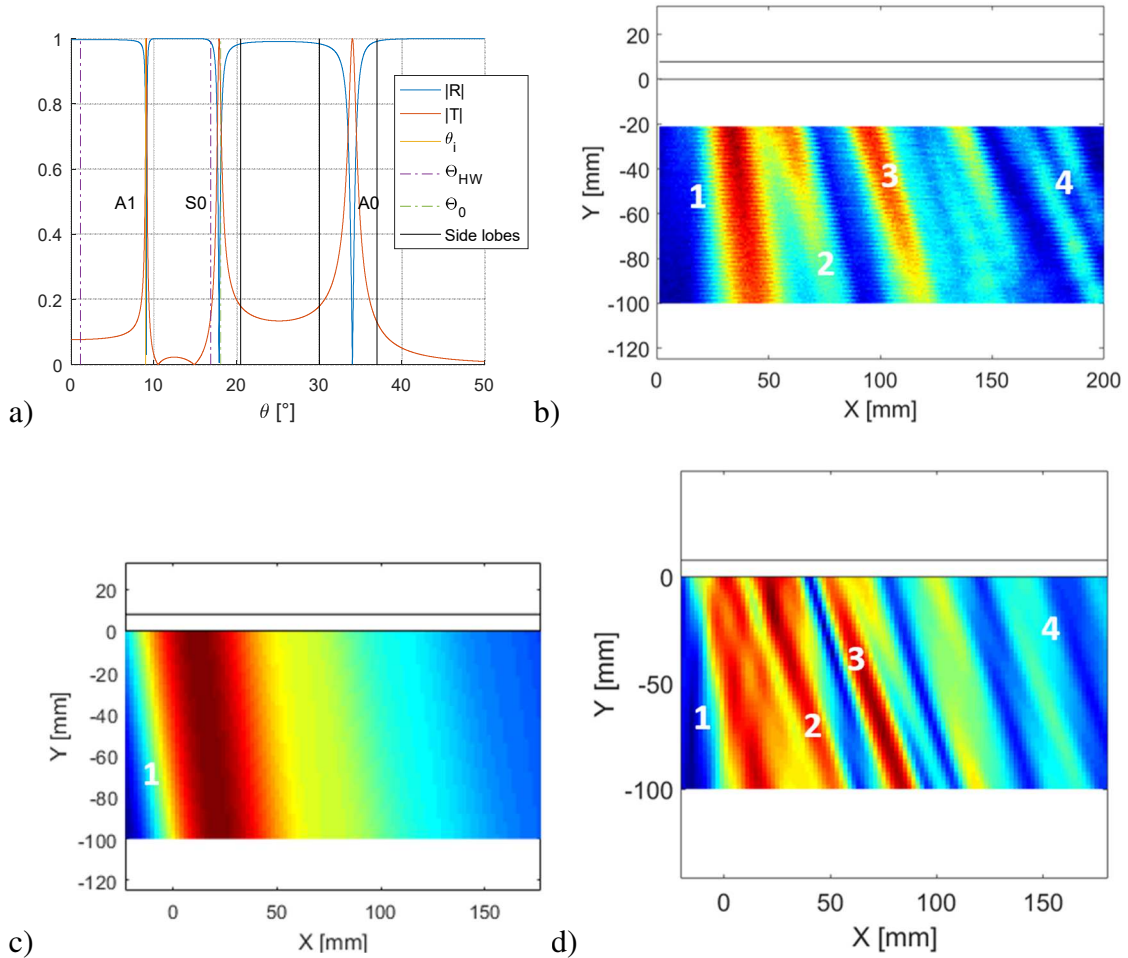
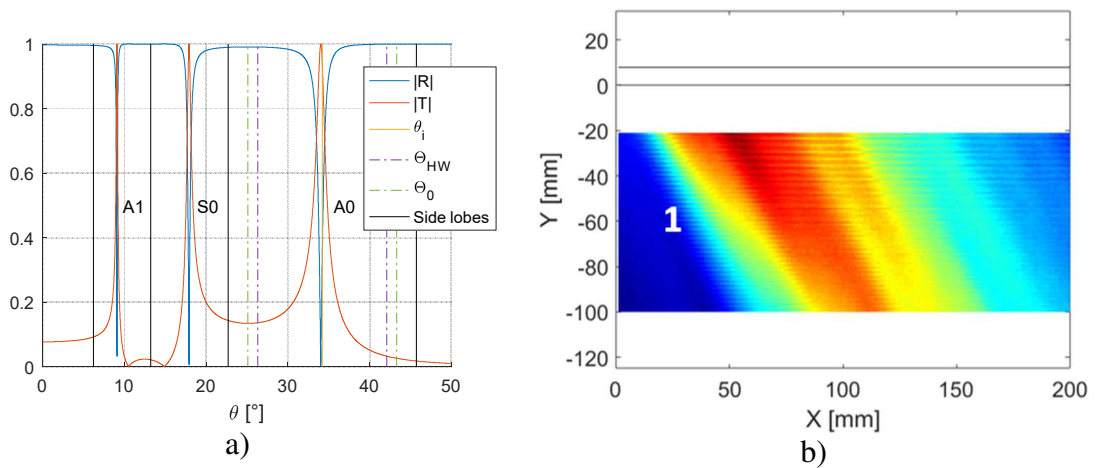


Figure 12: a) Reflection and transmission modulus with superposition of the main beam spreading angles Θ_{HW} and Θ_0 and incidence angles of side lobes for $\theta = 9^\circ$ at 250kHz. Comparison of the transmitted field: b) experimental C-scan, c) initial Bertoni and Tamir model and d) modified Bertoni and Tamir model with side lobes taken into account

Finally, the A0 mode has been targeted at $= 34.2^\circ$: this mode has a leaky attenuation close to S0 but both are higher than A1. The Figure 13.a shows that the main beam excites only the A0 mode, and that S0 and A1 can be excited by the three left side lobes. We can expect small interferences with S0 and negligible interferences with A1.

The initial Bertoni and Tamir model (Figure 13.c) only predict the re-emission of A0 (labelled 1) at 34° as expected. This direction was also measured on the experimentation (Figure 13.b) and with our modified Bertoni and Tamir model (Figure 13.d). However it is difficult to measure other directions Figure 13.b and Figure 13.d because the re-emitted field is distorted by interferences of small amplitudes, probably with the S0 mode.



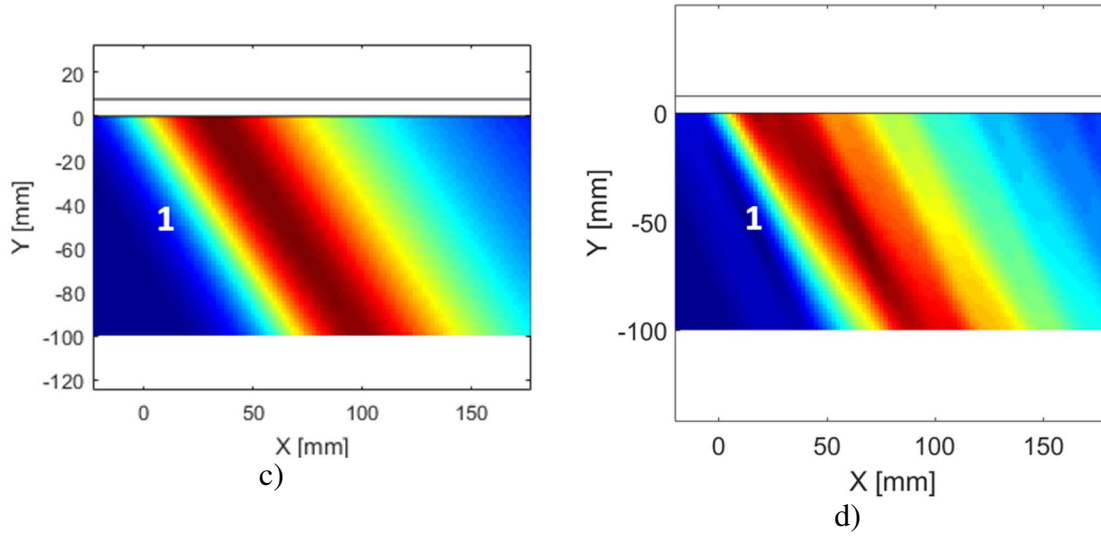


Figure 13: a) Reflection and transmission modulus with superposition of the main beam spreading angles θ_{HW} and θ_0 and incidence angles of side lobes for $\theta = 34.2^\circ$ at 250 kHz. Comparison of the transmitted field: b) experimental C-scan, c) initial Bertoni and Tamir model and d) modified Bertoni and Tamir model with side lobes taken into account

4. CONCLUSION

The analytical Bertoni and Tamir model is modified to take into account side lobes inherent to an experimental transducer. A finite-element simulation was also ran with the same incident bounded beam and validated these two techniques by experimental observation. We confirm the importance of taking the side lobes of the incident acoustic beam into account, in order to model correctly the re-emitted field that can present strong interferences in case of multimodal propagation. These interferences are predictable if the incident beam is well known.

When Lamb waves are used for NDT, it is usually better to excite a single Lamb mode for clarity of signals. Moreover, as a function of the defect, the creation of others Lamb modes can occur when the incident Lamb mode is reflecting on the defect. To avoid initial multi-modal propagation, one could suppress side lobes by using a

nonuniform transducer: such a transducer has his piezo-electric disk dividing into two zones, enabling a mean windowing of the initial excitation [33,34]. However, we can reduce the effect of side lobes on the plate by aiming with the main beam the leaky Lamb mode with the highest leaky attenuation coefficient. Others leaky Lamb modes are harder to be generated [16] and are likely to be negligible if a side lobe excites them. However, such highly attenuated modes are bad candidates for long range inspection of immersed plate. There is a compromise to be found case by case regarding the length of the plate to be controlled and the purity of the Lamb mode excited.

If multiple Lamb modes are generated by the only main beam, we could also increase its directivity by increasing the transducer diameter. Another way to achieve this goal is to use higher frequencies (some MHz) with thinner plates (few millimetres) as in [28]: the main incident beam will have better directivity, and Lamb modes will be easily decoupled from each other.

The finality of this work will be to achieve NDT in several parallel and immersed plates. To reach this goal, a complete study of leaky Lamb waves that propagates in two parallel and immersed plate is available in [35], and experimental detection of defects in the second plate are compared with theory in [36].

Acknowledgements

This research was supported by the CEA Cadarache centre, France.

Appendix: Properties of the plate and water used for numerical applications

The immersed plate is homogeneous, elastic and isotropic in stainless steel (density of $7\,950\text{ kg}\cdot\text{m}^{-3}$, longitudinal and shear velocities respectively of $5\,750\text{ m}\cdot\text{s}^{-1}$ and $3\,150\text{ m}\cdot\text{s}^{-1}$), with no attenuation due to the material (absorption and scattering). These values were measured on the stainless steel plate used for experimentation.

Water is modelled with a density of $1\,000\text{ kg}\cdot\text{m}^{-3}$ and a speed of sound equal to $1\,490\text{ m}\cdot\text{s}^{-1}$. The viscosity of water is neglected.

References

- [1] F. Jadot, F. Baqué, J.P. Jeannot, G. de Dinechin, J.M. Augem, J. Sibilo, ASTRID sodium cooled fast reactor: Program for improving in service inspection and repair, in: 2011 2nd International Conference on Advancements in Nuclear Instrumentation, Measurement Methods and Their Applications (ANIMMA), 2011: pp. 1–8. doi:10.1109/ANIMMA.2011.6172910.
- [2] F. Baqué, F. Jadot, R. Marlier, J.F. Saillant, V. Delalande, In Service Inspection and Repair of the sodium cooled ASTRID reactor prototype, in: Proceedings of ICAPP'15, Nice, France, 2015.
- [3] G. Corneloup, M.-A. Ploix, J.-F. Chaix, I. Lillamand, F. Baqué, Potential of Ultrasounds for NDT of a structure located behind parallel immersed plates, in: Review of Progress in Quantitative NonDestructive Evaluation: Volume 30A; Volume 30B, AIP Publishing, 2011: pp. 1695–1700. doi:10.1063/1.3592132.
- [4] P. Kauffmann, M.-A. Ploix, J.-F. Chaix, C. Gueudré, G. Corneloup, F. Baqué, Study of Lamb Waves for Non-Destructive Testing Behind Screens, in: 2017 5th International Conference on Advancements in Nuclear Instrumentation, Measurement Methods and Their Applications (ANIMMA), EPJ Web of Conferences, Liège, Belgium, 2018. doi:10.1051/epjconf/201817003005.
- [5] D. Alleyne, P. Cawley, Optimization of lamb wave inspection techniques, NDT & E International. 25 (1992) 11–22. doi:10.1016/0963-8695(92)90003-Y.
- [6] D. Alleyne, P. Cawley, The Interaction of Lamb Waves with Defects, IEEE Trans. Ultrason. Ferroelectr. Freq. Control. 39 (1992) 381–397. doi:10.1109/58.143172.
- [7] A.H. Nayfeh, Wave propagation in layered anisotropic media: with applications to composites, Elsevier, Amsterdam ; New York, 1995.

- [8] P. Wilcox, M. Lowe, P. Cawley, Lamb and SH wave transducer arrays for the inspection of large areas of thick plates, in: AIP, 2000: pp. 1049–1056. doi:10.1063/1.1306159.
- [9] M. Castaings, E. Le Clezio, B. Hosten, Modal decomposition method for modeling the interaction of Lamb waves with cracks, The Journal of the Acoustical Society of America. 112 (2002) 2567–2582. doi:10.1121/1.1500756.
- [10] I.A. Viktorov, Rayleigh and Lamb Waves: Physical Theory and Applications, Softcover reprint of the original 1st ed. 1967 edition, Springer, 2013.
- [11] A.H. Nayfeh, P.B. Nagy, Excess attenuation of leaky Lamb waves due to viscous fluid loading, The Journal of the Acoustical Society of America. 101 (1997) 2649–2658. doi:10.1121/1.418506.
- [12] L.G. Merkulov, Damping of normal modes in a plate immersed in a liquid, Sov. Phys. Acoust. 10 (1964) 169–173.
- [13] A.E. Takiy, C. Kitano, R.T. Higuti, S.C.G. Granja, V.T. Prado, L. Elvira, O. Martinez-Graullera, Ultrasound imaging of immersed plates using high-order Lamb modes at their low attenuation frequency bands, Mech. Syst. Signal Proc. 96 (2017) 321–332. doi:10.1016/j.ymssp.2017.04.021.
- [14] A. Bernard, M.J.S. Lowe, M. Deschamps, Guided waves energy velocity in absorbing and non-absorbing plates, J. Acoust. Soc. Am. 110 (2001) 186–196. doi:10.1121/1.1375845.
- [15] D.E. Chimenti, S.I. Rokhlin, Relationship between leaky Lamb modes and reflection coefficient zeroes for a fluid-coupled elastic layer, The Journal of the Acoustical Society of America. 88 (1990) 1603–1611. doi:10.1121/1.400319.

- [16] P.D. Wilcox, M.J.S. Lowe, P. Cawley, Mode and transducer selection for long range lamb wave inspection, *J. Intell. Mater. Syst. Struct.* 12 (2001) 553–565. doi:10.1106/N9PB-Y62E-P0Y2-50QF.
- [17] A. Pilarski, J.J. Ditri, J.L. Rose, Remarks on symmetric Lamb waves with dominant longitudinal displacements, *The Journal of the Acoustical Society of America*. 93 (1993) 2228–2230. doi:10.1121/1.406684.
- [18] H.L. Bertoni, T. Tamir, Unified theory of Rayleigh-angle phenomena for acoustic beams at liquid-solid interfaces, *Applied Physics*. 2 (1973) 157–172. doi:10.1007/BF00884205.
- [19] P.D. Wilcox, M.J.S. Lowe, P. Cawley, The effect of dispersion on long-range inspection using ultrasonic guided waves, *NDT & E International*. 34 (2001) 1–9. doi:10.1016/S0963-8695(00)00024-4.
- [20] Y.-F. Xu, W.-X. Hu, Wideband dispersion removal and mode separation of Lamb waves based on two-component laser interferometer measurement, *Chin. Phys. B*. 26 (2017) 094301. doi:10.1088/1674-1056/26/9/094301.
- [21] C. Potel, S. Baly, J.F. de Belleval, M. Lowe, P. Gagniol, Deviation of a monochromatic Lamb wave beam in anisotropic multilayered media: Asymptotic analysis, numerical and experimental results, *IEEE Trans. Ultrason. Ferroelectr. Freq. Control*. 52 (2005) 987–1001. doi:10.1109/TUFFC.2005.1504021.
- [22] J. Rautenberg, S. Olfert, F. Bause, B. Henning, Validation of analytically modeled Leaky Lamb radiation using Schlieren photography, in: *Ultrasonics Symposium (IUS)*, 2012 IEEE International, 2012: pp. 819–822. doi:10.1109/ULTSYM.2012.0204.

- [23] N.F. Declercq, J. Degrieck, O. Leroy, Bounded Beam Interaction with Plate-Edge at Lamb Angle, *Acta Acustica United with Acustica*. 91 (2005) 326–332.
- [24] M. Schmitt, K. Schmidt, S. Olfert, J. Rautenberg, G. Lindner, B. Henning, L.M. Reindl, Detection of coatings within liquid-filled tubes and containers by mode conversion of leaky Lamb waves, *Journal of Sensors and Sensor Systems*. 2 (2013) 73–84. doi:10.5194/jsss-2-73-2013.
- [25] T.J. Plona, L.E. Pitts, W.G. Mayer, Ultrasonic bounded beam reflection and transmission effects at a liquid/solid-plate/liquid interface, *The Journal of the Acoustical Society of America*. 59 (1976) 1324–1328. doi:10.1121/1.381011.
- [26] L.E. Pitts, T.J. Plona, W.G. Mayer, Theory of Nonspecular Reflection. Effects for an Ultrasonic Beam Incident on a Solid Plate in a Liquid, *IEEE Transactions on Sonics and Ultrasonics*. 24 (1977) 101–108. doi:10.1109/T-SU.1977.30919.
- [27] T.D.K. Ngoc, W.G. Mayer, A General Description of Ultrasonic Nonspecular Reflection and Transmission Effects for Layered Media, *IEEE Transactions on Sonics and Ultrasonics*. 27 (1980) 229–235. doi:10.1109/T-SU.1980.31182.
- [28] T.D.K. Ngoc, W.G. Mayer, Influence of Plate Mode Structure and Gaussian Beam Profile Characteristics on Ultrasonic Reflection and Transmission, *IEEE Transactions on Sonics and Ultrasonics*. 29 (1982) 112–114. doi:10.1109/T-SU.1982.31316.
- [29] M. Aanes, K.D. Lohne, P. Lunde, M. Vestrheim, Beam Diffraction Effects in the Backward Wave Regions of Viscoelastic Leaky Lamb Modes for Plate Transmission at Normal Incidence, *IEEE Trans. Ultrason. Ferroelectr. Freq. Control*. 64 (2017) 1558–1572. doi:10.1109/TUFFC.2017.2719627.
- [30] D.T. Blackstock, *Fundamentals of physical acoustics*, Wiley, New York, 2000.

- [31] B. Moudjed, Experimental and theoretical characterization of acoustic streaming. Prospect of an use for photovoltaic Silicon solidification., Theses, INSA de Lyon, 2013. <https://tel.archives-ouvertes.fr/tel-00958258> (accessed January 3, 2017).
- [32] M. Castaings, C. Bacon, B. Hosten, M.V. Predoi, Finite element predictions for the dynamic response of thermo-viscoelastic material structures, J. Acoust. Soc. Am. 115 (2004) 1125–1133. doi:10.1121/1.1639332.
- [33] D. De Vadder, A. Lhémy, N. Gengembre, A New Ultrasonic Transducer Combining Three Modes: High Axial Resolution, High Transverse Resolution and Standard Modes, in: Review of Progress in Quantitative Nondestructive Evaluation: Volume 15A, Springer US, Boston, MA, 1996: pp. 979–986. doi:10.1007/978-1-4613-0383-1_128.
- [34] A. Lhémy, D. De Vadder, N. Gengembre, Wideband Nonuniformly Excited Focused Transducers - Theory and Experiments, in: Review of Progress in Quantitative Nondestructive Evaluation: Volume 15A, Springer US, Boston, MA, 1996: pp. 963–970. doi:10.1007/978-1-4613-0383-1_126.
- [35] P. Kauffmann, M.-A. Ploix, J.-F. Chaix, C. Gueudré, G. Corneloup, F. Baqué, Multi-modal leaky Lamb waves in two parallel and immersed plates: theoretical considerations, simulations and measurements, The Journal of The Acoustical Society of America. 145 (2019) 1018-1030. doi: 10.1121/1.5091689
- [36] P. Kauffmann, M.-A. Ploix, J.-F. Chaix, C. Gueudré, G. Corneloup, F. Baqué, Non-Destructive Testing of Nuclear Structures behind Screen using Leaky Lamb Waves, in: 45th Annual Review of Progress in Quantitative Nondestructive Evaluation, AIP, Conference Proceedings, Burlington, USA, 2018.

Collected figure captions

Figure 1: Experimental bench: incident bulk waves are sent by a transducer onto a plate immersed in water (7.8 mm thick and 700 mm long). Leaky Lamb waves are generated (symbolized by dashed blue arrow), and the transmitted acoustic field (bold red arrows) is scanned by a needle hydrophone in an area perpendicular to the plate (dash-dotted yellow line).

Figure 2: a) Theoretical reflection and transmission modulus at 500 kHz of the immersed stainless-steel plate as a function of the incidence angle θ . b) Theoretical leaky attenuation coefficient of Lamb modes for a stainless-steel plate with a thickness of 7.8 mm.

Figure 3: An example of a transmitted beam profile with representation of the main acoustic beam spreading phenomena

Figure 4: a) Reflection and transmission modulus with superposition of the main beam spreading angles Θ_{HW} and Θ_0 and incidence angles of side lobes for $\theta = 30.4^\circ$ at 500kHz. Comparison of the transmitted field: b) experimental C-scan, and c) Bertoni and Tamir model. The plate is illustrated by two parallel black lines and is immersed on both sides.

Figure 5: a) Reflection and transmission modulus with superposition of the main beam spreading angles Θ_{HW} and Θ_0 and incidence angles of side lobes for $\theta = 17.2^\circ$ at 500kHz. Comparison of the transmitted field: b) experimental C-scan, and c) Bertoni and Tamir model, with d) extracted normalised amplitude for $Y = -20$ mm.

Figure 6: Transmitted acoustic field in our configuration computed with the FEM: the absolute pressure is plotted in water and vertical displacements in the plate

Figure 7: Experimental characterisation of the incident acoustic beam used in our configuration. The red line shows the near field length, representing also the mean abscissa where the plate is located during experimentation

Figure 8: Incident acoustic beam profile with superposition of different model: the Bertoni and Tamir modelling (Gaussian) and optimised least-squares models (Bessel Cardinal and Lorentz functions)

Figure 9: a) Transmitted acoustic field in our configuration computed with the modified Bertoni and Tamir model. b) Reflection and transmission modulus with superposition of the main beam spreading angles Θ_{HW} and Θ_0 and incidence angles of side lobes. c) Comparison of the amplitude at $Y = -20$ mm for the experimentation and the Bertoni and Tamir model with and without side lobes implementation.

Figure 10: Comparison of the transmitted field on the same scale: a) experimental C-scan, b) finite-element simulation and c) modified analytical Bertoni and Tamir model

Figure 11: Experimental characterisation of the incident acoustic beam used at 250 kHz. The red line shows the near field length, representing the mean abscissa where the plate is located during experimentation

Figure 12: a) Reflection and transmission modulus with superposition of the main beam spreading angles Θ_{HW} and Θ_0 and incidence angles of side lobes for $\theta = 9^\circ$ at 250kHz. Comparison of the transmitted field: b) experimental C-scan, c) initial Bertoni and Tamir model and d) modified Bertoni and Tamir model with side lobes taken into account

Figure 13: a) Reflection and transmission modulus with superposition of the main beam spreading angles Θ_{HW} and Θ_0 and incidence angles of side lobes for $\theta = 34.2^\circ$ at 250

651 kHz. Comparison of the transmitted field: b) experimental C-scan, c) initial Bertoni and
652 Tamir model and d) modified Bertoni and Tamir model with side lobes taken into
653 account

654

655

656 **Collected table captions**

657 Table 1: Piecewise definition of θ_n for X positive. The definition of θ_n for X
658 negative is based on the same scheme, with directions symmetrical to θ

659